2012 IEEE/RSJ International Conference on
Intelligent Robots and Systems
October 7-12, 2012. Vilamoura, Algarve, Portugal

Interaction Force Estimation During Manipulation of Microparticles

Islam S. M. Khalil*, Roel M. P. Metz*, Leon Abelmann† and Sarthak Misra*
University of Twente, The Netherlands

Abstract— **This work investigates the utilization of microparticles for the wireless sensing of interaction forces in magnetic-based manipulation systems. The proposed force estimation approach allows for using microparticles in sensing the interaction forces at hard-to-reach regions to avoid the mechanical and electronic complexities associated with physical force sensors. Based on the velocity of the microparticle and the applied currents at each of the electromagnets of the magnetic system, an interaction force observer is designed to estimate the contact forces between the microparticle and a soft-tissue simulant with different elasticities. Experimentally, a magnetic system is utilized to steer a microparticle towards a soft-tissue simulant to carry out force sensing. The experimental results show that forces in the range of nano-Newton can be estimated without nano-force sensors. The estimated interaction forces due to this contact can be used either in sensing and diagnosis applications, or in the realization of a force control system.**

I. INTRODUCTION

Limited minimally invasive surgical interventions can be carried out by microparticles, which can be steered and controlled by the influence of the applied magnetic fields [1]-[3]. Such interventions require sensing the interaction forces between the microparticles and their surrounding tissues [4]. This requirement necessitates the utilization of force sensors to provide reliable functionality. However, it is hard to embed force sensors to microparticles or microrobots due to their associated mechanical and electronic complexities along with their size. Generally, force sensors sense the strain capacitively, peizoresistively, peizoelectrically or optically; and hence they are unsuitable for *in vivo* interventions. Therefore, we attempt to utilize microparticles in sensing and diagnosis of diseased hard-to-reach regions via a wireless magnetic system (the force estimation approach is implemented on the magnetic system shown in Fig. 1). The size of these microparticles, which ranges from 30 μm to 100 μm, would allow them to be used in large arteries of the human blood circulatory system (diameters range from 1.0 mm to 4.0 mm) [5]. In addition, microparticles under the influence of magnetic field benefit from the wireless power transmission along with the transparency of the human body (permeability of the human body is almost the same as that of the vacuum) [6], hence their capability to access hard-to-reach regions within the human body.

Much effort has been expended to sense or estimate interaction forces at micro- or nano-scales [7]-[9]. A microrobotic system for grasping of biological cells at nano-Newton force level was achieved based on employing a microgripper that integrates two-axis force sensors for resolving the gripping and contact forces between a gripping arm and a substrate [10]. A two-axis force sensor was optimized to maximize sensitivity and bandwidth for the characterization of microrobots [11]. However, it depends on capacitively sensing the strain and converting it into force signal via calibration operation and therefore it is difficult to be utilized *in vivo*. A six-axis force-torque sensor intended for microrobotic applications was designed and fabricated [12], [13]. Its probe is 3 mm long and the size of the sensor chip is $10 \times 9 \times 0.5$ mm^3, which limits its operating range. A three-axes miniaturized bulk micro-machined piezoresistive force sensor was developed and has the advantage of providing high sensitivity and high resonance frequencies [14]. However, its size ($6.5 \times 6.5 \times 0.25$ mm^3) could possibly limit its operating range, e.g., the size of this force sensor exceeds the largest arteries of the human blood circulatory system (4 mm in diameter).

There is a body of work related to the micromanipulation and control of microparticles and microrobots by the applied

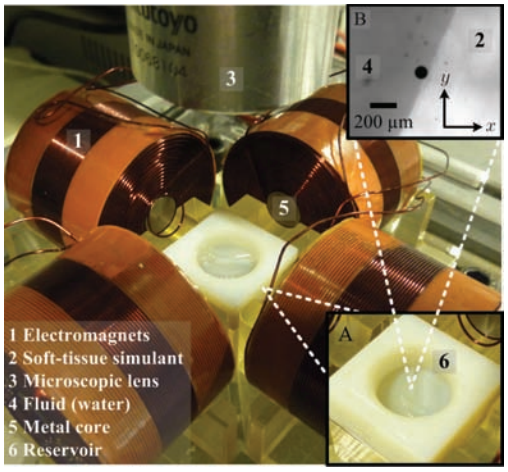

Fig. 1. Magnetic system developed for the wireless control of microparticles [21]. The microparticle is used to sense the interaction forces with a soft-tissue simulant. Inset A shows a reservoir which contains a fluid and a soft-tissue simulant that possesses the mechanical properties of the biological tissue. Inset B shows a 100 μm spherical microparticle in contact with the soft-tissue simulant. The magnetic system can be used for wireless manipulation, sensing and diagnosis by the applied magnetic fields at each of the metal-core electromagnets.

*Islam S. M. Khalil, Roel M. P. Metz and Sarthak Misra are with MIRA–Institute for Biomedical Technology and Technical Medicine.
†Leon Abelmann is with MESA+ Institute for Nanotechnology.
{i.s.m.khalil,l.abelmann,s.misra}@utwente.nl
r.m.p.metz@student.utwente.nl

TABLE I

EXPERIMENTAL PARAMETERS

Parameter	Value	Parameter	Value
r_p	50×10^{-6} m	μ_0	$4\pi \times 10^{-7}$T.m/A
η	1 mPa.s	g	30 rad/s
ρ	998.2 kg.m^{-3}	$k_{p1} = k_{p2}$	15.0 s^{-2}
χ	0.17 ± 0.007	$k_{d1} = k_{d2}$	5.0 s^{-1}
M	7.33×10^{-10}kg	E_{s1}	35 kPa
E_{s2}	$\sim$ 70 kPa		

magnetic fields [15]-[18]. Kummer *et al.* [19], presented a 5-DOF wireless magnetic system for controlling an untethered microrobot within a large workspace for delicate retinal applications. An electromagnetic system was presented in [20], where magnetic propulsion was utilized to move a 3 mm ferromagnetic thermoseed to reach a brain tumour. The proposed wireless force sensing approach allows for using the aforementioned magnetic systems in sensing the interaction forces without any additional sensors or major modifications.

This work analyzes an approach for the wireless magnetic-based estimation of the interaction forces between microparticles and their surrounding environment. This approach avoids the mechanical and electronics complexities associated with force sensors. In addition, it provides microparticles or microrobots with wide range of applications since no extra force sensors have to be embedded to their structure. The analyzed approach demonstrates the possibility of estimating contact forces in the range of few nano-Newton up to tens of nano-Newton. While the experiments presented in this work are based on visual feedback, the wireless magnetic-based force sensing approach could be used for sensing *in vivo* provided that a suitable imaging technique is available.

The remainder of this paper is organized as follows: Section II provides the theoretical background pertaining to modeling of the contact mechanism between a microparticle in a fluid and a soft-tissue simulant under the influence of magnetic fields. The design of the interaction force observer is provided in Section III. In Section IV, the experimental validation is conducted on a magnetic system and a soft-tissue simulant with different elasticities. Finally, Section V concludes and provides directions for future work.

II. FORCES ACTING ON MICROPARTICLES

Utilization of microparticles in minimally invasive surgical interventions depends on their ability to apply calibrated and well-controlled forces. In this section, the contact between a microparticle and an environment is analyzed. The impedance (Z_t) of the environment is assumed unknown. The interaction force ($\mathbf{F_{ext}} \in \mathbb{R}^{3\times1}$) due to the contact with this environment is given by

$$\mathbf{F_{ext}} = Z_t \mathbf{X_t} = (K_t + sD_t)\mathbf{X_t}, \tag{1}$$

where $\mathbf{X_t} \in \mathbb{R}^{3\times1}$ is the position response vector of the environment. Further, K_t and D_t are its stiffness and damping coefficients, respectively. In order to sense the interaction forces, we have to model the contact between the microparticle and the environment. In the presence of a driving magnetic force ($\mathbf{F(P)} \in \mathbb{R}^{3\times1}$) and a drag ($\mathbf{F_d} \in \mathbb{R}^{3\times1}$), the motion equation of the microparticle is given by

$$\mathbf{F(P)} - \mathbf{F_d} - \mathbf{F_{ext}} = \mathrm{M}\ddot{\mathbf{P}}, \tag{2}$$

where M and $\mathbf{P} \in \mathbb{R}^{3\times1}$ are the mass and position vector of the microparticle, respectively. The surrounding fluid in which the microparticle navigates has the following Reynolds number (R_e) [23]

$$R_e = \frac{2\rho v r_p}{\eta}, \tag{3}$$

where ρ, v, r_p and η are the microparticle density, velocity, radius and fluid dynamic viscosity, respectively. Due to the properties of the surrounding fluid (parameters are provided in Table I) and the velocity and size of the microparticle, Reynolds number is low ($<< 0.1$). Therefore, the magnitude of the drag force (F_d) is

$$F_d = 6\pi\eta r_p v. \tag{4}$$

Due to the influence of the applied magnetic fields, the microparticle experiences a driving magnetic force given by

$$\mathbf{F(P)} = \nabla\left(\mathbf{m(P)} \cdot \mathbf{B(P)}\right) = \frac{4}{3}\frac{1}{\mu}\pi r_p^3 \chi_m \nabla\left(\mathbf{B}^2\mathbf{(P)}\right), \tag{5}$$

where $\mathbf{m(P)} \in \mathbb{R}^{3\times1}$ and $\mathbf{B(P)} \in \mathbb{R}^{3\times1}$ are the induced magnetic dipole moment of the microparticle and the induced magnetic field, respectively. Further, μ is the permeability coefficient given by, $\mu = \mu_0(1 + \chi_m)$. Moreover, μ_0 and χ_m are the vacuum permeability and magnetic susceptibility constants, respectively [24]. The magnetic field is related to

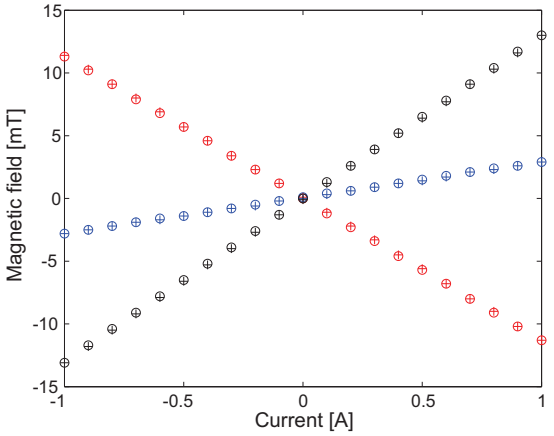

Fig. 2. Experimental validation of the current-magnetic field linearity and hysteresis. Components of the magnetic field at a representative point (10 mm along the centerline and from the side of one of the electromagnets shown in Fig. 1) within the workspace of the system are plotted versus the increasing (denoted by $\circ$) and decreasing (denoted by $+$) current. The red, blue and black colors represent the magnetic field components along x-, y- and z-axis, respectively. The magnetic fields are generated by metal-core electromagnets and measured by a calibrated three-axis Hall magnetometer (Sentron AG, Digital Teslameter 3MS1-A2D3-2-2T, Switzerland).

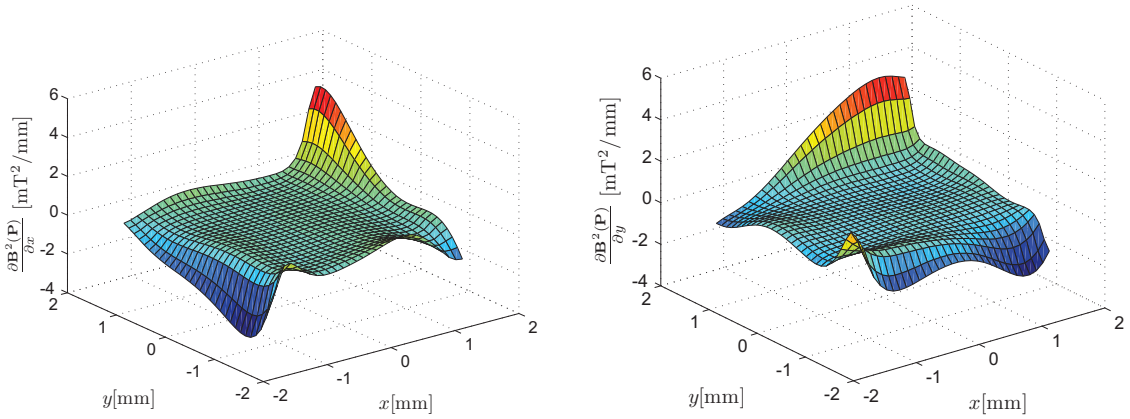

(a) Gradient of the magnetic field square along x-axis

(b) Gradient of the magnetic field square along y-axis

Fig. 3. The gradient of the magnetic field square along x- and y-axis. The finite element (FE) analysis describes the magnetic field behavior within a workspace of 2×2 mm^2 when a current vector of $[0.1\ 0.2\ 0.3\ 0.4]^{\mathrm{T}}$ A is applied. The gradients are almost constant within the workspace of our system, therefore the matrix $(\nabla(\widetilde{\mathbf{B}}^{\mathrm{T}}(\mathbf{P})\widetilde{\mathbf{B}}(\mathbf{P})))$ does not have to be calculated at each point of the workspace. Gradients are calculated by a FE model for the magnetic system shown in Fig. 1. The FE model is created using Comsol Multiphysics® (COMSOL, Inc., Burlington, U.S.A).

the applied currents at each of the n-electromagnets of the system (with metal cores) by the following relation [19]

$$\mathbf{B}(\mathbf{P}) = \widetilde{\mathbf{B}}(\mathbf{P})\mathbf{I}, \tag{6}$$

where $\widetilde{\mathbf{B}}(\mathbf{P}) \in \mathbb{R}^{3\times n}$ and $\mathbf{I} \in \mathbb{R}^{n\times 1}$ are the position dependent constant matrix and current input vector, respectively. Linearity of the field-current relation (6) is verified experimentally. The magnetic field is measured using a three-axis Hall magnetometer (Sentron AG, Digital Teslameter 3MS1-A2D3-2-2T, Switzerland), and plotted versus the increasing and decreasing current input (Fig. 2). Substituting (6) in (5) yields the following force-current map:

$$\mathbf{F}(\mathbf{P}) = \frac{4}{3}\frac{1}{\mu}\pi r_p^3 \chi_m \mathbf{I}^{\mathrm{T}} \left(\nabla\left(\widetilde{\mathbf{B}}^{\mathrm{T}}(\mathbf{P})\widetilde{\mathbf{B}}(\mathbf{P})\right)\right)\mathbf{I}. \tag{7}$$

The mapping (7) can be used as a basis of the open- and closed-loop control of microparticles. Its inverse has to be realized when it is required to calculate the currents from the desired forces. In our case, where the interaction forces are required to be estimated, the forward force-current map (7) is utilized. It is important to note that the matrix $(\nabla(\widetilde{\mathbf{B}}^{\mathrm{T}}(\mathbf{P})\widetilde{\mathbf{B}}(\mathbf{P})))$ has almost a constant value within a limited region of the workspace of the system. The gradient of the magnetic field square along x- and y-axis are provided in Figs. 3(a) and (b), respectively, for the magnetic system shown in Fig. 1. This observation simplifies the implementation of the interaction force observer since we no longer need to compute the matrix $(\nabla(\widetilde{\mathbf{B}}^{\mathrm{T}}(\mathbf{P})\widetilde{\mathbf{B}}(\mathbf{P})))$ at each point of the workspace illustrated in Fig. 3.

III. INTERACTION FORCE OBSERVER

Sensing is accomplished by pushing the microparticle with the magnetic forces against an environment, then the interaction forces during transient and steady state are observed from the available measurements of the magnetic system, i.e, the velocity of the microparticle and the applied currents. Based on (2), we devise an observer of the following form [25], [26]:

$$\dot{\widehat{\mathbf{F}}}_{\mathbf{ext}} = -g\widehat{\mathbf{F}}_{\mathbf{ext}} + g\left[\mathbf{F}(\mathbf{P}) - \mathrm{M}\ddot{\mathbf{P}} - \mathbf{F_d}\right], \tag{8}$$

where $\widehat{\mathbf{F}}_{\mathbf{ext}} \in \mathbb{R}^{3\times 1}$ is the estimated interaction force, and $g \in \mathbb{R}^+$ is the cut-off frequency of the low-pass filter associated with the interaction force observer. The force estimation error ($\mathbf{e_f} = \mathbf{F_{ext}} - \widehat{\mathbf{F}}_{\mathbf{ext}}$) can be determined from (2) and (8). Therefore, we obtain the following force estimation error dynamics:

$$\dot{\mathbf{e}}_{\mathbf{f}} = \dot{\mathbf{F}}_{\mathbf{ext}} - \dot{\widehat{\mathbf{F}}}_{\mathbf{ext}}. \tag{9}$$

The interactions between the microparticle and the soft-tissue simulant are assumed to vary slowly ($\dot{\mathbf{F}}_{\mathbf{ext}} = 0$). Therefore, using (2), (8) and (9), the force estimation error dynamics is

$$\dot{\mathbf{e}}_{\mathbf{f}} + g\mathbf{e_f} = 0, \tag{10}$$

which indicates that the estimated interaction force will converge to the actual one in finite time. Nevertheless, we define auxiliary functions to avoid realizing the estimated interaction force through the acceleration of the microparticle

$$\mathbf{\Gamma} = \widehat{\mathbf{F}}_{\mathbf{ext}} - \Phi(\dot{\mathbf{P}}), \tag{11}$$

where $\mathbf{\Gamma}$ and $\Phi(\dot{\mathbf{P}})$ are auxiliary functions. In (11), $\mathbf{\Gamma}$ provides a change of variables to avoid measuring the acceleration of the microparticle, whereas $(\Phi(\dot{\mathbf{P}}))$ is a function (to be determined) of the velocity of the microparticle. The time derivative of (11) is

$$\dot{\mathbf{\Gamma}} = \dot{\widehat{\mathbf{F}}}_{\mathbf{ext}} - \frac{\partial \Phi(\dot{\mathbf{P}})}{\partial \dot{\mathbf{P}}}\ddot{\mathbf{P}}. \tag{12}$$

Substituting (11) and (12) in (8) yields

$$\dot{\mathbf{\Gamma}} + \frac{\partial \Phi(\dot{\mathbf{P}})}{\partial \dot{\mathbf{P}}}\ddot{\mathbf{P}} = g\left[\mathbf{F}(\mathbf{P}) - \mathrm{M}\ddot{\mathbf{P}} - \mathbf{F_d} - \mathbf{\Gamma} - \Phi(\dot{\mathbf{P}})\right]. \tag{13}$$

Setting the auxiliary function, $\frac{\partial \Phi(\dot{\mathbf{P}})}{\partial \dot{\mathbf{P}}} = -g\mathrm{M}$, yields the following representation of the interaction force observer in terms of the auxiliary function ($\mathbf{\Gamma}$):

$$\dot{\mathbf{\Gamma}} = g\left[\mathbf{F}(\mathbf{P}) - \mathbf{F_d} - \mathbf{\Gamma} - \Phi(\dot{\mathbf{P}})\right]. \tag{14}$$

By taking the Laplace transform of (14)

$$\mathbf{\Gamma} = \frac{g}{s+g}\left[\mathbf{F}(\mathbf{P}) - \mathbf{F_d} - \Phi(\dot{\mathbf{P}})\right]. \tag{15}$$

Finally, substituting (15) in (11) yields

$$\widehat{\mathbf{F}}_{\mathbf{ext}} = \frac{g}{s+g}\left[\mathbf{F}(\mathbf{P}) - \mathbf{F_d} - \Phi(\dot{\mathbf{P}})\right] + \Phi(\dot{\mathbf{P}}). \tag{16}$$

From (16), estimating the interaction force ($\widehat{\mathbf{F}}_{\mathbf{ext}}$) requires measuring the velocity of the microparticle and the input current vector ($\mathbf{F}(\mathbf{P})$ can be represented explicitly in terms of ($\mathbf{I}$) using the forward force-current map (7)). In addition, the nominal parameters of the fluid must be known beforehand. The interaction force observer is illustrated in Fig. 4. It is worth noting that the cut-off frequency of the observer (g) controls the convergence speed of the estimated interaction force to the actual one. However, its value is limited by the bandwidth of the position or velocity sensor noise. The performance of the interaction force observer depends on the quality of the measured or estimated velocity. In general, the dominating forces in micromanipulation of biological cells are in the range of hundreds nano-Newton up to hundreds of micro-Newton. Therefore, if the velocity measurement is noisy, the observer would fail to provide reliable estimates. In our work, the velocity of the microparticle is determined by differentiating the position measurement through a low-pass filter. The interaction force observer benefits from the low frequency range at which manipulation of microparticles generally occurs by filtering the high frequency noise without affecting the performance.

IV. EXPERIMENTAL WORK

In order to analyze the implementation of the interaction force observer, experiments are conducted on the magnetic system shown in Fig. 1, which consists of an orthogonal array of four metal-core electromagnets. The array surrounds a fluid reservoir in which the microparticle is immersed. The reservoir contains water and soft-tissue simulant. Position of the microparticle is determined by means of a microscopic system that is mounted on the top of the reservoir and a feature tracking software [21]-[22]. The microparticles utilized throughout our experimental work are paramagnetic, consisting of iron-oxide in a poly (lactic acid) matrix (PLA-Particles-M-redF-plain from Micromod Partikeltechnologie GmbH, Rostock-Warnemuende, Germany). The experimental parameters are provided in Table I.

First, the motion of the microparticle is controlled towards an environment (soft-tissue simulant composed of gelatine). Hereafter, the interaction forces between the microparticle and the soft-tissue simulant are estimated by (16). It is worth mentioning that the interaction force observer relies on a single measurement from the magnetic system (velocity of the microparticle), as the currents at each of the electromagnets are known inputs. In order to steer the microparticle towards the soft-tissue simulant or any point within the workspace of the magnetic system, the following control input is applied:

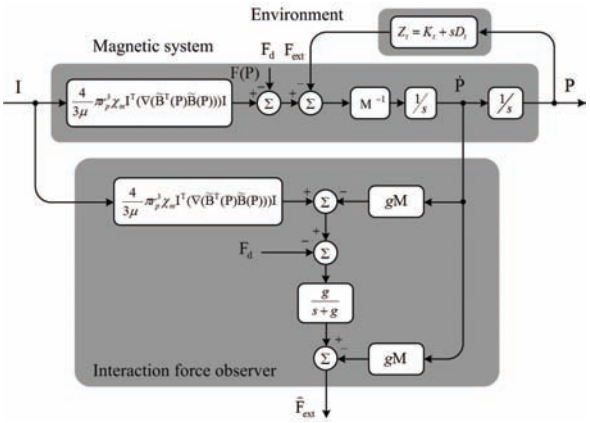

Fig. 4. Interaction force observer for the estimation of the contact forces between a microparticle and the surrounding environment. The impedance (Z_t) of the environment is unknown, whereas the properties of the fluid are known beforehand. The interaction force observer requires measuring the velocity of the microparticle ($\dot{\mathbf{P}}$) along with the applied current ($\mathbf{I}$). The force-current map (7) generated by the finite element analysis is used in the realization of the interaction force observer. Assuming that the gradients of the field square are almost constant within the workspace of the magnetic system (as shown in Fig. 3), simplifies the force-current map as the matrix ($\nabla(\tilde{\mathbf{B}}^{\mathrm{T}}(\mathbf{P})\tilde{\mathbf{B}}(\mathbf{P}))$) no longer has to be calculated at each point of the workspace. The magnetic, drag and contact forces are $\mathbf{F}(\mathbf{P})$, $\mathbf{F_d}$ and $\mathbf{F_{ext}}$, respectively. The estimated contact force is $\widehat{\mathbf{F}}_{\mathbf{ext}}$, and g is the scalar gain of the interaction force observer.

$$\mathbf{F}(\mathbf{P}) = \mathbf{F_d} + \mathrm{M}\left(\ddot{\mathbf{P}}_{ref} - \mathbf{K_d}\dot{\mathbf{e}} - \mathbf{K_p}\mathbf{e}\right), \tag{17}$$

where $\ddot{\mathbf{P}}_{ref}$ is the desired acceleration reference input. Further, $\dot{\mathbf{e}} = \dot{\mathbf{P}}_{ref} - \dot{\mathbf{P}}$ is the velocity tracking error of the microparticle and similarly, $\mathbf{e} = \mathbf{P}_{ref} - \mathbf{P}$ is the position tracking error (velocity of the microparticle is calculated by taking the derivative of the position vector through a low-pass filter with a cut-off frequency of 30 rad/s). Moreover, $\mathbf{P}_{ref}$ and $\dot{\mathbf{P}}_{ref}$ are the position and velocity reference vectors, respectively. The controller gain matrices, ($\mathbf{K_p}$ and $\mathbf{K_d}$) must achieve stable position error tracking dynamics through the proper selection and tuning of

$$\mathbf{K_p} = \begin{bmatrix} k_{p1} & 0 \\ 0 & k_{p2} \end{bmatrix} \text{ and } \mathbf{K_d} = \begin{bmatrix} k_{d1} & 0 \\ 0 & k_{d2} \end{bmatrix}, \tag{18}$$

where k_{pi} and k_{di}, for $(i = 1, 2)$, are the proportional and derivative gains, respectively. The position tracking experimental results using (17) are illustrated in Fig. 5. Tracking of multiple reference set points is achieved within the planar workspace of the magnetic system in the absence of contact with the soft-tissue simulant. Figs. 5(a) and (b) illustrate the planar motion of the microparticle along x- and y-axis versus the time, respectively. The controller gains are provided in Table I.

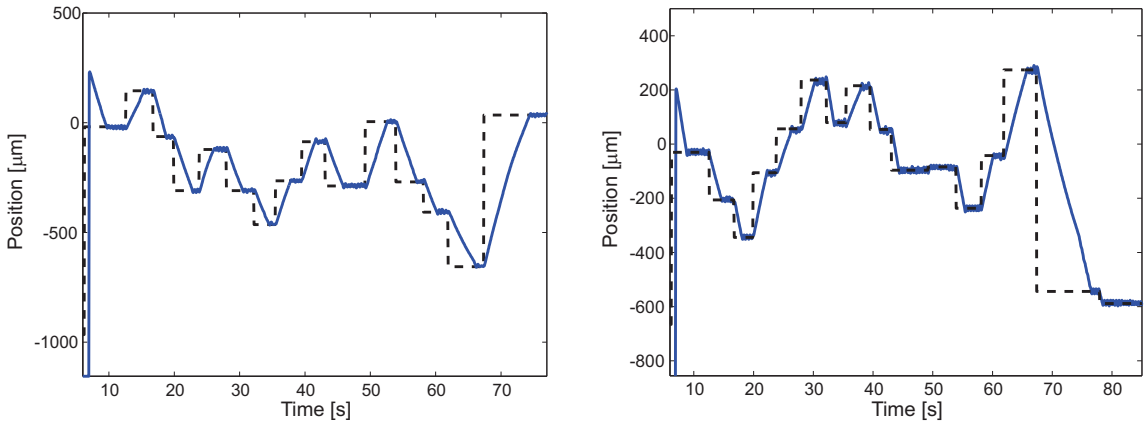

(a) Microparticle position along x-axis

(b) Microparticle position along y-axis

Fig. 5. Motion control experimental results of a microparticle under the influence of the applied magnetic fields in the absence of contact with the soft-tissue simulant. The microparticle tracks different points within the planar workspace of the magnetic system. The black dashed lines represent the reference set points along x-axis and y-axis, whereas the blue line represents the actual path taken by the controlled microparticle. The controller gains are: $k_{pi} = 15.5\ \mathrm{s}^{-2}$ and $k_{di} = 5.0\ \mathrm{s}^{-1}$ for $(i = 1, 2)$. This motion control result is accomplished by the control law (17).

The microparticle is steered towards the soft-tissue simulant using the motion control input (17). Fig. 6(a) illustrates the contact between the microparticle and the soft-tissue simulant, whereas the actual path taken by the microparticle is illustrated in Fig. 6(b). The experimental results of the force estimation are provided in Figs. 7(a) and (b) for the estimated interaction forces along x- and y-axis, respectively. In this experiment, the microparticle is steered towards the soft-tissue simulant (gelatine) and the interaction force components are observed. This experiment is conducted on gelatine with elasticity (E_{s1}) of 35 kPa, the estimated interaction force components are provided with the black lines in Figs. 7(a) and (b). In addition, we estimate the interaction force components for another soft-tissue simulant with elasticity E_{s2}. The value of E_{s2} is almost twice E_{s1} to examine the functionality of the observer for environments with various elasticities. The estimated force components are provided with the blue dashed lines in Figs. 7(a) and (b).

The interaction force observer estimates contact forces in the range of tens of nano-Newton during the initial contact between the microparticle and the soft-tissue simulant as shown in Figs. 7(a) and (b). The force peaks shown in Figs. 7(a) and (b), indicate the initial contact forces along x- and y-axis, respectively, when the microparticle is moving with an average velocity of 130 μm/s towards the soft-tissue simulant. In the steady state, the observer estimates forces in the range of few nano-Newton (shown in the magnified plots of Figs. 7(c) and (d)) during the attempt of the microparticle to reach a reference position which is given inside the soft-tissue simulant. Therefore, the outlined magnetic-based estimation approach can be utilized during the characterization of biological cells and general micromanipulation operations.

The analyzed interaction force observer is not verified by comparing the estimated forces with the measured ones due to the unavailability of force sensors that can be immersed in the fluid and provide force measurements without affecting the magnetic fields. However, we implement the interaction force observer on two environments with different elasticities and the corresponding estimated forces are proportional to the elasticities of the soft-tissue simulant. We provide a proof-of-concept for the estimation of the interaction forces during the wireless manipulation of microparticles and microrobots. The outlined interaction force observer along with the magnetic wireless manipulation system can be utilized as a wireless force sensor providing a wide range of applications due to the miniaturized size of the microparticle and the simplicity of the magnetic system.

V. CONCLUSIONS AND FUTURE WORK

In minimally invasive surgical interventions with biological tissue and micromanipulation of biological cells, interaction forces have to be sensed and often feedback to provide reliable functionality. Embedding force sensors with microparticles or microrobots would limit their operating range due to the size of the force sensors along with their associated mechanical and electronic complexities. In this work, we analyze an approach for the estimation of the interaction forces between microparticles and the surrounding environment. The contact forces are estimated by an interaction force observer which is designed based on the velocity of the microparticle and the applied currents at each of the electromagnets of the magnetic system. Experimentally, a soft-tissue simulant is used as the surrounding environment. A magnetic system which has been developed for the purpose of manipulation of microparticles is then used to steer a microparticle towards this soft-tissue simulant. The magnetic system is utilized as a wireless force sensor since it can estimate the contact forces between the navigating microparticle (or microrobot) and its surrounding environment. This work demonstrates that microparticles or microrobots can be used

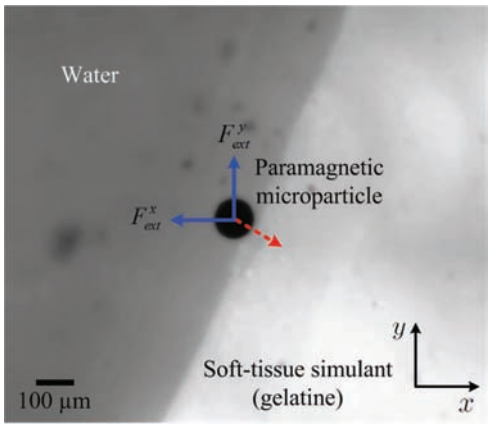

(a) Contact of the microparticle with the soft-tissue simulant

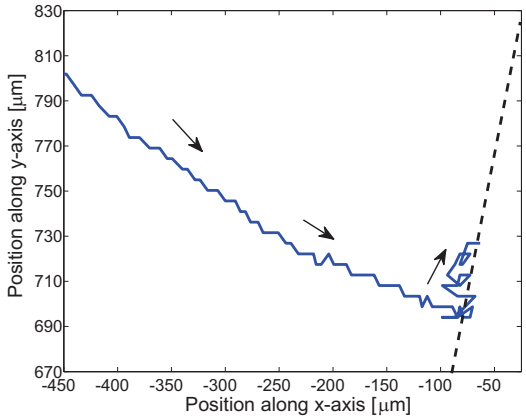

(b) Motion of microparticle towards the soft-tissue simulant

Fig. 6. Microparticle interacting with a soft-tissue simulant by the influence of the applied magnetic fields generated by the electromagnets. (a) Microparticle in contact with the soft-tissue simulant. The red dashed arrow indicates the direction of motion for the microparticle, whereas the blue arrows represent symbolically the interaction force components (F^x_{ext} and F^y_{ext}). (b) The microparticle moves towards the soft-tissue simulant, then it exhibits a motion (sliding) along the edge of the soft-tissue simulant. This sliding motion is due to the presence of a position reference beyond the edge of the soft-tissue simulant. The blue line indicates the path taken by the microparticle during the force sensing experiment. The black arrows indicate the direction of the microparticle. The black dashed lines represent the edge of the soft-tissue simulant. The controller gains are: $k_{pi} = 15.5\ \mathrm{s}^{-2}$ and $k_{di} = 5.0\ \mathrm{s}^{-1}$ for $(i = 1, 2)$. This motion control result is accomplished by the control law (17), while the interaction forces are simultaneously estimated using the interaction force observer (16). *Please refer to the attached video that demonstrates the results of the interaction force estimation experiment.*

for sensing forces in the range of few nano-Newton without force sensors. Therefore, they could be used to sense and impose forces in this range during diagnosis and limited invasive surgical interventions, respectively.

As future work, calibration of the outlined wireless magnetic-based force estimation system will be conducted. This calibration requires developing a precise custom-built force sensing system which does not perturb the magnetic fields during the force measurement (this is not the case with most of the commercial nano-force sensors). In addition, the force sensing system will be optimized for measurement inside fluidic bodies and provide force measurement in the nano-Newton range. Moreover, The proposed approach will be used to perform sensing and diagnosis *in vivo*, provided that a suitable imaging technique is employed and integrated with the interaction force observer.

REFERENCES

[1] J.-B. Mathieu and S. Martel, "Steering of aggregating magnetic microparticles using propulsion gradients coils in an MRI scanner," *Magnetic Resonance in Medicine*, vol. 63, no. 5, pp. 1336-1345, May 2010.

[2] J.-B. Mathieu and S. Martel, "Magnetic steering of iron oxide microparticles using proulsion gradient ciols in MRI," in *Proceedings of the International Conference of the IEEE Engineering in Medicine and Biology Society (EMBS)*, pp. 472-475, New York City, USA, September 2006.

[3] S. S. Shevkoplyas, A. C. Siegel, R. M. Westervelt, M. G. Prentiss, and G. M. Whitesides, "The force acting on a superparamagnetic bead due to an applied magnetic field," *Lab on a Chip*, vol. 7, no. 6, pp. 1294-1302, July 2007.

[4] S. J. Koch, G. E. Thayer, A. D. Corwin, and M. P. de Boer, "Micromachined piconewton force sensor for biophysics investigations," *Applied Physics Letters*, vol. 89, no. 17, pp. 173901 - 173901-3, October 2006.

[5] S. Martel, J.-B. Mathieu, O. Felfoul, H. Macicior, G. Beaudoin, G. Soulez, and L. Yahia, "Adapting MRI systems to propel and guide microdevices in the human blood circulatory system," in *Proceedings of the International Conference of the IEEE Engineering in Medicine and Biology Society (EMBS)*, pp. 1044-1047, San Francisco, USA, September 2004.

[6] B. J. Nelson, I. K. Kaliakatsos, and J. J. Abbott, "Microrobots for minimally invasive medicine," *The Annual Review of Biomedical Engineering*, vol. 12, pp. 55-85, April 2010.

[7] S. Fahlbusch and S. Fatikow, "Force sensing in microrobotic systems–an overview," in *Proceedings of the IEEE International Conference on Electronics, Circuits and Systems (ICECS)*, vol. 3, pp. 259-262, Lisboa, Portugal, September 1998.

[8] J. J. Abbott, Z. Nagy, F. Beyeler, and B. J. Nelson, "Robotics in the small, part I: microbotics," *IEEE Robotics and Automation Magazine*, vol. 14, no. 2, pp. 92-103, June 2007.

[9] L. Dong and B. J. Nelson, "Tutorial-Robotics in the small part II: nanorobotics," *IEEE Robotics and Automation Magazine*, vol. 14, no. 3, pp. 111-121, September 2007.

[10] X. Liu, K. Kim, Y. Zhang, and Y. Sun, "Nanonewton force sensing and control in microrobotic cell manipulation," *The International Journal of Robotics Research*, vol. 28, no. 8, pp. 1065-1076, August 2009.

[11] R. J. Wood, K-J. Cho, and K. Hoffman, "A novel multi-axis force sensor for microrobotics applications," *Smart Materials and Structures*, vol. 18, pp. 1-7, September 2009.

[12] F. Beyeler, S. Muntwyler, and B. J. Nelson, "Design and calibration of a microfabricated 6-axis force-torque sensor for microrobotic applications," in *Proceedings of the IEEE International Conference on Robotics and Automation (ICRA)*, pp. 520-525, Kobe, Japan, May 2009.

[13] F. Beyeler, S. Muntwyler, Z. Nagy, C. Graetzel, M. Moser, and B. J. Nelson, "Design and calibraion of a MEMS sensor for measuring the force and torque acting on a magnetic microrobot," *Journal of Micromechanics and Microengineering*, vol. 18, pp. 1-7, December 2007.

[14] A. Tibrewala, A. Phataralaoha, and S. Buttgenbach, "Simulation, fabrication and characterization of a 3D piezoresistive force sensor," *Sensors and Actuators*, vol. 147, no. 2, pp. 430-435, October 2008.

[15] J.-B. Mathieu, S. Martel, L. Yahia, G. Soulez, and G. Beaudoin, "MRI systems as a mean of propulsion for a microdevice in blood vessels," in *Proceedings of the International Conference of the IEEE Engineering in Medicine and Biology Society (EMBS)*, vol. 4, pp. 3419-3422, Cancun, Mexico, September 2003.

[16] D. C. Meeker, E. H. Maslen, R. C. Ritter, and F. M. Creighton, "Optimal realization of arbitrary forces in a magnetic stereotaxis

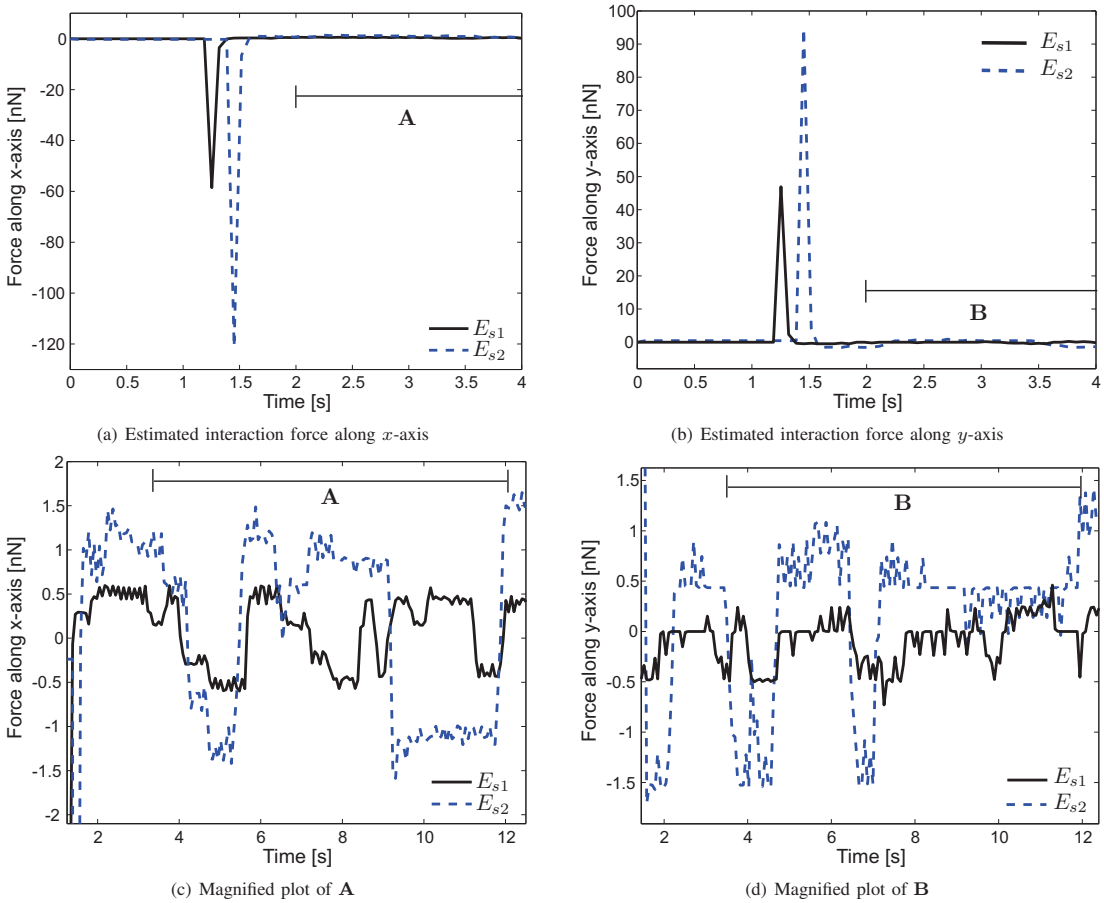

(a) Estimated interaction force along x-axis

(b) Estimated interaction force along y-axis

(c) Magnified plot of **A**

(d) Magnified plot of **B**

Fig. 7. Interaction force estimation experimental results. The interaction forces due to the contact of the microparticle with the soft-tissue simulant are estimated along x- and y-axis using the interaction force observer (16). The microparticle is steered towards the soft-tissue simulant using the position control law (17) then the contact forces are estimated. The black lines indicate the estimated force components during the contact between the microparticle and the soft-tissue simulant with elasticity (E_{s1}) of 35 kPa, whereas the blue dashed lines indicate the estimated interaction force components for a simulant that has almost twice the elasticity of the first. The estimated forces can be used in the realization of the force control by microparticles and microrobots to avoid the mechanical and electronic complexities associated with physical force sensors. The controller gains are: $k_{pi} = 15.5$ s^{-2} and $k_{di} = 5.0$ s^{-1} for $(i = 1, 2)$, whereas the gain of the interaction force observer is: $g = 30$ rad/s. This force estimation result is accomplished by the control law (17) and the interaction force observer (16). *Please refer to the attached video that demonstrates the results of the interaction force estimation experiment.*

system," *IEEE Transactions on Magnetics*, vol. 32, no. 2, pp. 320-328, March 1996.

[17] J. J. Abbott, O. Ergeneman, M. P. Kummer, A. M. Hirt, and B. J. Nelson, "Modeling magnetic torque and force for controlled manipulation of soft-magnetic bodies," *IEEE Transactions on Robotics and Automation*, vol. 23, no. 6, pp. 1247-1252, December 2007.

[18] G. T. Gillies, R. C. Ritter, W. C. Broaddus, M. S. Grady, M. A. Howard, and R. G. McNeil, "Magnetic manipulation instrumentation for medical physics research, "*Review of Scientific Instruments*, vol. 65, no. 3, pp. 533-562, March 1994.

[19] M. P. Kummer, J. J. Abbott, B. E. Kartochvil, R. Borer, A. Sengul, and B. J. Nelson, "OctoMag: an electromagnetic system for 5-DOF wireless micromanipulation," *IEEE Transactions on Robotics*, vol. 26, no. 6, pp. 1006-1017, December 2010.

[20] R. G. McNeil, R. C. Ritter, B. Wang, M. A. Lawson, G. T. Gillies, K. G. Wika, E. G. Quate, M. A. Howard, and M. S. Grady, "Characteristics of an improved magnetic-implant guidance system," *IEEE Transactions on Biomedical Engineering*, vol. 42, no. 8, pp. 802-808, August 1995.

[21] J. D. Keuning, J. de Vries, L. Abelmann, and S. Misra, "Image-based magnetic control of paramagnetic microparticles in water," in *Proceedings of the IEEE/RSJ International Conference of Robotics and Systems (IROS)*, pp. 421-426, San Francisco, USA, September 2011.

[22] I. S. M. Khalil, J. D. Keuning, L. Abelmann, and S. Misra, "Wireless magnetic-based control of paramagnetic microparticles," in *Proceedings of the IEEE RAS/EMBS International Conference on Biomedical Robotics and Biomechatronics (BioRob)*, pp. 460-466, Rome, Italy, June 2012.

[23] K. B. Yesin, K. Vollmers, and B. J. Nelson, "Modeling and control of untethered biomicrorobots in a fluidic environment using electromagnetic fields," *International Journal of Robotics Research*, vol. 25, no. 4-5, pp. 527-536, May 2006.

[24] B. D. Cullity and C. D. Graham, "Introduction to magnetic materials,", 2nd ed. *Hoboken, NJ: Wiley*, 2009.

[25] S. Komada, N. Machii, and T. Hori, "Control of redundant manipulators considering order of disturbance observer," *IEEE Transactions on Industrial Electronics*, vol. 47, no. 2, pp. 413-420, April 2000.

[26] S. Katsura, Y. Matsumoto, and K. Ohnishi, "Modeling of force sensing and validation of disturbance observer for force control," *IEEE Transactions on Industrial Electronics*, vol. 54, no. 1, pp. 530-538, February 2007.